Sectorized Antenna-based DoA Estimation and Localization: Advanced Algorithms and Measurements

Janis Werner, *Student Member, IEEE*, Jun Wang, Aki Hakkarainen, *Student Member, IEEE*, Nikhil Gulati, *Student Member, IEEE*, Damiano Patron, *Student Member, IEEE*, Doug Pfeil, Kapil Dandekar, *Senior Member, IEEE*, Danijela Cabric, *Senior Member, IEEE*, and Mikko Valkama, *Member, IEEE*

***Abstract*—Sectorized antennas are a promising class of antennas for enabling direction-of-arrival (DoA) estimation and successive transmitter localization. In contrast to antenna arrays, sectorized antennas do not require multiple transceiver branches and can be implemented using a single RF front-end only, thus reducing the overall size and cost of the devices. However, for good localization performance the underlying DoA estimator is of uttermost importance. In this paper, we therefore propose a novel high performance DoA estimator for sectorized antennas that does not require cooperation between the transmitter and the localizing network. The proposed DoA estimator is broadly applicable with different sectorized antenna types and signal waveforms, and has low computational complexity. Using computer simulations, we show that our algorithm approaches the respective Cramer-Rao lower bound for DoA estimation variance if the signal-to-noise ratio (SNR) is moderate to large and also outperforms the existing estimators. Moreover, we also derive analytical error models for the underlying DoA estimation principle considering both free space as well as multipath propagation scenarios. Furthermore, we also address the fusion of the individual DoA estimates into a location estimate using the Stansfield algorithm and study the corresponding localization performance in detail. Finally, we show how to implement the localization in practical systems and demonstrate the achievable performance using indoor RF measurements obtained with practical sectorized antenna units.**

***Index Terms*—Angle-of-arrival, cognitive radio, directional antennas, direction-of-arrival estimation, leaky-wave antennas, localization, location-awareness, measurements, reconfigurable antennas, sectorized antennas, Stansfield algorithm.**

I. Introduction

TRANSMITTER (TX) localization has many application areas [1], [2]. In many of those areas, it is desired that the TX location is estimated based on observing or measuring the transmission alone, without any direct collaboration or feedback signaling between the TX and localization network. In cognitive radio networks, as an example, the primary user (PU) cannot be expected to cooperate with the secondary network. Nevertheless, PU location information has been identified as one of the key requirements to enable several advanced functionalities in cognitive radio networks [2]. Other good examples of TX localization are spectrum enforcement, surveillance, first responder operations as well as transportation and navigation.

The location of a non-cooperative TX can generally be estimated by measuring time-difference-of-arrival (TDoA) [3], received-signal-strength (RSS) [4], [5], direction-of-arrival (DoA) [6] or combinations thereof [7], [8]. However, TDoA measurements require accurate timing synchronization in the localizing network itself [7]. In order to avoid the increased complexity associated with synchronization, most recent research has therefore focused on RSS [4], [5] and DoA-based localization [6]–[8]. Intuitively and as shown also in, e.g., [6]–[8], the accuracy of DoA-based localization systems is strongly determined by the quality of DoA estimates. Therefore, this paper will thoroughly investigate advanced DoA estimation algorithms and their application and performance in localization systems.

Traditional approaches of DoA estimation such as the popular MUSIC algorithm [9] require digitally controlled antenna arrays (DCAA). For accurate DoA estimation, the DCAAs must be equipped with a large number of antennas, each with a complete receiver branch [10]. However, the associated hardware complexity of such an implementation might be infeasible in handheld devices. We have therefore recently proposed to use so-called sectorized antennas for DoA estimation [11]–[13]. A sectorized antenna is an abstraction that encompasses all types of antennas that can receive energy selectively within an angular sector. Thereby, it is not required that different sectors

Manuscript received August 15, 2014; revised December 7, 2014; accepted January 11, 2015. Date of publication May 6, 2015; date of current version October 19, 2015. This work was supported by the Doctoral Program of the President of Tampere University of Technology, the Tuula and Yrjö Neuvo Fund, the Nokia Foundation, the Academy of Finland under the project 251138 "Digitally-Enhanced RF for Cognitive Radio Devices," and the Finnish Funding Agency for Technology and Innovation (Tekes, under the projects "Reconfigurable Antenna-based Enhancement of Dynamic Spectrum Access Algorithms," "5G Networks and Device Positioning," and "Future Small-Cell Networks using Reconfigurable Antennas").

J. Werner, A. Hakkarainen, and M. Valkama are with the Department of Electronics and Communications Engineering, Tampere University of Technology, Tampere FI-33101, Finland (e-mail: janis.werner@tut.fi; aki.hakkarainen@tut.fi; mikko.e.valkama@tut.fi).

J. Wang and D. Cabric are with the Department of Electrical Engineering, University of California, Los Angeles, CA 90095 USA (e-mail: eejunwang@ucla.edu; danijela@ee.ucla.edu).

N. Gulati, D. Patron, D. Pfeil, and K. Dandekar are with the Department of Electrical and Computer Engineering, Drexel University, Philadelphia, PA 19104 USA (e-mail: ng54@drexel.edu; dp578@drexel.edu; dsp36@drexel.edu; krd26@drexel.edu).

Color versions of one or more of the figures in this paper are available online at http://ieeexplore.ieee.org.

Digital Object Identifier 10.1109/JSAC.2015.2430292

can receive the signal in a time-parallel manner. Sectorized antennas can, consequently, be implemented with a single RF front-end only and are therefore generally much less hardware-intensive than DCAAs. Practical examples of sectorized antennas are reconfigurable antennas such as leaky-wave antennas (LWAs) [14] or electronically steerable parasitic array radiators (ESPARs) [15] as well as switched-beam systems (SBSs) [16] or antenna arrays with a single RF front-end [17], [18].

In the literature, various DoA estimators for sectorized antennas have been proposed. However, most of these estimators were developed for a specific type of sectorized antenna and some are moreover restricted to specific signal types or require a cooperating TX. In [19] the angle-dependent frequency response of an LWA is exploited to estimate the DoA of a wideband pulsed signal. The algorithms in [15], [20], [21] require a cooperating TX that sends the same signal repeatedly, such that the signal is received in all sectors of an ESPAR [15] or an LWA [20], [21]. In that way, the antennas can be used to emulate a DCAA and subsequent MUSIC DoA estimation becomes possible. DoA estimation of multiple DS-CDMA signals impinging on a base station equipped with an SBS is considered in [16]. However, the estimator in [16] requires either the RSS to be known or an additional omnidirectional antenna at the receiver in order to normalize the received signals properly. In [22], [23] different DoA estimators for antenna arrays with a single RF front-end are compared based on simulations with advanced propagation modeling [22], [23] and open field measurements [23]. Analog DoA estimation with an LWA is proposed in [24]. Since the estimation is performed by continuously changing the antenna's beam, the algorithm is not applicable to all sectorized antennas. In addition, the associated measurement process takes longer time than a measurement in sectors (i.e., in discrete steps). In [11], [22], [25] an estimator is considered that estimates the DoA as the orientation of the sector with the maximum power measurement. In accordance with [11], we refer to this algorithm as the maxE estimator. While maxE has very low computational complexity, its performance is ultimately limited by the number of sectors and is far from the performance bounds as discussed in detail in [11] and [12].

Another DoA estimator for sectorized antennas, namely the simplified least squares (SLS) estimator, was proposed in [12]. SLS builds on the assumption that only a few sectors receive the TX signal at a sufficiently high SNR, while the attenuation in the other sectors is too high to exploit the TX signal component. Based on this assumption, SLS measures the powers in all sectors and discards all sector-powers except for the maximum two. The ratio of the two remaining sector-powers is then used in a least-squares formulation to estimate the DoA. SLS has been shown to outperform the estimators in [11], [25], and also closely approaches the Cramer-Rao bound (CRB) for moderate SNRs [12]. However, for high SNRs the performance of SLS saturates and does not achieve the CRB. In addition, our analysis in [12] assumes a somewhat optimal beamwidth for the antenna's main beam. This optimal beamwidth decreases with the number of sectors. However, in practice it is often impossible to change the beamwidth, which is determined by the underlying antenna technology. Instead, the only way to improve DoA estimation performance is to increase the number of sectors while keeping the beamwidth constant. Consequently, the assumption that all but two sectors can be discarded in DoA estimation does not apply for a number of practical scenarios, which severely degrades the performance of SLS DoA estimation for all SNRs. Moreover, the estimators in [11], [12], [25], require a sectorized antenna where the main beam is equally shaped in all sectors. In practice this is not necessarily the case as is evident, e.g., from the LWA in [14].

In this paper, we therefore propose, analyze and test the three-stage SLS (TSLS) DoA estimator for sectorized antennas. TSLS does not make any assumptions about the TX signal, nor does it require sectors with equally shaped radiation patterns. We only require that the main beam of the radiation pattern can be roughly approximated by a Gaussian-shaped curve, an approximation that has been shown feasible for a large number of antennas [11], [26], [27]. For the proposed estimator, we then shown that its performance closely approaches the respective CRB for moderate to large SNR. Finally, this paper demonstrates the application of TSLS in a practical localization system that computes a TX location estimate from TSLS DoA estimates obtained at multiple sensors.

In detail, our contributions in this paper are the following:

- Generalization of the model for sectorized antennas in [11] such that it is also applicable to sectorized antennas where the shape of the main beam varies throughout the sectors.
- We propose and analyze the universal and high-performance TSLS DoA estimator for sectorized antennas. TSLS computes the DoA in three stages. First, TSLS selects the sectors suitable for DoA estimation. Using pairs of these sectors, TSLS subsequently estimates sector-pair DoAs (SP-DoAs) that are then fused together to obtain the final DoA estimate.
- We develop different methods for SP-DoA fusion.
- We derive analytical error models for bias and variance of SP-DoA estimates.
- We analyze the effects of multipath on the underlying DoA estimation principle both analytically and through simulations.
- We study in detail the performance of a complete localization system where TSLS DoA estimates from multiple sensors are combined into a TX location estimate by means of the modified Stansfield algorithm.
- We apply TSLS DoA estimation in practice and demonstrate the achievable localization performance with real-world RF measurements that were obtained in an indoor environment.

This paper is organized as follows. Section II describes the localization system and the sectorized antenna model. The TSLS estimator is introduced in Section III, while the analytical error models for SP-DoA estimation are derived in Section IV. The Stansfield localization algorithm is briefly reviewed in Section V. A thorough performance and complexity evaluation of DoA estimation and localization with TSLS through computer simulations and practical measurements can be found in Section VI and Section VII, respectively. The work is

TABLE I
MOST COMMONLY USED ABBREVIATIONS

CRB	Cramer-Rao bound	PW	power weighting	RSS	received-signal-strength
DBS	different beamwidth sectors	VW	variance weighting	RX/TX	receiver/transmitter
DCAA	digitally controlled antenna arrays	LS	least squares	SBS	switched beam system
		LWA	leaky-wave antenna	SDE	sector-pair DoA estimation
DFU	DoA fusion	MASP	maximum adjacent sector-pair	SLS	simplified least squares
DoA	direction-of-arrival			SNR	signal-to-noise ratio
EBS	equal beamwidth sectors	NCSP	noise-centered sector-powers	SSL	sector selection
ESA	equal sector antenna			SP-DoA	sector-pair DoAs
EW	equal weighting	RMSE	root mean squared error	TSLS	three-stage SLS

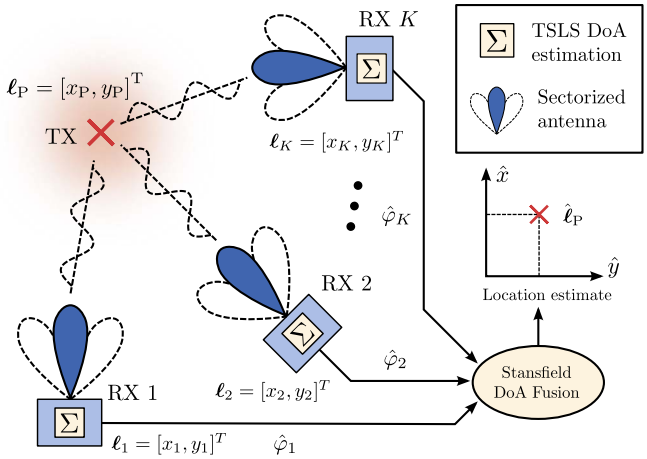

Fig. 1. Considered localization system with K RX units and a single TX.

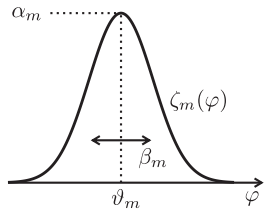

Fig. 2. An illustration of the antenna model (1) for sector m.

concluded in Section VIII. Details of derivations and proofs can be found in the Appendices A, B, and C.

Notation: Throughout this paper, vectors and matrices are written as bold letters. The absolute value of a complex number x is represented as $|x|$, the maximum of two real values x_1 and x_2 is written as $\max(x_1, x_2)$, and $\mathrm{mod}_y(x)$ expresses the remainder of the division x/y. $\mathrm{E}[X]$ and $\mathrm{var}[X]$ denote expected value and variance of the random variable X, while $\mathrm{bias}[\hat{y}] = \mathrm{E}[\hat{y}] - y$ denotes the bias of estimator $\hat{y}$ for a deterministic quantity y. $\mathrm{RMSE} = \sqrt{\mathrm{E}[\|\hat{\mathbf{y}} - \mathbf{y}\|^2]}$ denotes the root-mean squared error of an estimator $\hat{\mathbf{y}}$ for a deterministic vector (or scalar) $\mathbf{y}$, where $\|\mathbf{y}\|$ refers to the L^2 norm. We use $|A|$ to denote the cardinality of a set A. The superscripts $(\cdot)^T$ and $(\cdot)^{-1}$ represent transpose and matrix inverse, respectively. The trace of a matrix is expressed as $\mathrm{trace}(\mathbf{M})$, while $\mathrm{diag}(\mathbf{x})$ denotes the diagonal matrix with the elements of vector $\mathbf{x}$ on its diagonal. The symbol $\mathbf{e}_n$ is used to express a vector with 1 in the n-th coordinate and 0s otherwise. Finally, $X \sim \mathcal{N}(\mu_x, \sigma_x^2)$ denotes a Gaussian distributed real random variable with mean μ_x and variance σ_x^2 and $Z \sim \mathcal{CN}(\mu_z, \sigma_z^2)$ denotes a circular symmetric complex Gaussian distributed random variable with mean μ_z and variance σ_z^2.

For the readers' convenience, we have collected the most commonly used abbreviations in Table I.

II. SYSTEM MODEL

In this paper, we consider a localization system illustrated in Fig. 1. In this system, K receivers (RXs) with known locations $\boldsymbol{\ell}_k = [x_k, y_k]^{\mathrm{T}}$, $k = 1, \ldots, K$ collaborate in order to estimate the location, $\boldsymbol{\ell}_{\mathrm{P}} = [x_{\mathrm{P}}, y_{\mathrm{P}}]^{\mathrm{T}}$, of a non-cooperative TX. With the help of a sectorized antenna, each RX k estimates the TX signal DoA φ_k using the algorithm we propose in Section III. Thereafter, the DoA estimates from all RXs are communicated to a central fusion center, where they are combined into a TX location estimate $\hat{\boldsymbol{\ell}}_{\mathrm{P}} = [\hat{x}_{\mathrm{P}}, \hat{x}_{\mathrm{P}}]^T$ using a modified version of the Stansfield algorithm [11], [28] (see Section V).

As discussed in [11], [26], [27], the main beam of many directional antennas can be well approximated through a Gaussian-like shape. Here, we consider a generalized radiation pattern model that has more degrees of freedom compared to our earlier model (e.g., [11]). Consequently, this new model is well suited for a broader range of practical antennas.

Assume that each sensor is capable of taking measurements in M different sectors. The radiation pattern of sector m, $m = 1, \ldots, M$ is then modeled as

$$\zeta_m(\varphi) = \alpha_m \exp\left(-\left[\mathcal{M}(\varphi - \vartheta_m)\right]^2 / \beta_m^2\right) \tag{1}$$

where β_m is the beamwidth of the main beam, ϑ_m is the orientation and α_m is the attenuation of the antenna in sector m, and $\mathcal{M}(\varphi) = \mathrm{mod}_{2\pi}(\varphi + \pi) - \pi$. An illustration of (1) can be found in Fig. 2. The TSLS DoA estimator, proposed in Section III, estimates SP-DoAs using measurements from two sectors. Hence, for a given sector pair (i, j), $i, j = 1, \ldots, M$, we distinguish between two cases: 1) equal beamwidth sectors (EBS): $\beta_i = \beta_j$ and 2) different beamwidth sectors (DBS): $\beta_i \neq \beta_j$. This distinction is necessary since EBS and DBS require different SP-DoA estimators as will be shown in Section III-B. From (1), the earlier model in [11] is obtained when $\alpha_i = \alpha_j = 1$, $\beta_i = \beta_j$ and $|\Delta\vartheta_{ij}| = |\vartheta_i - \vartheta_j| = \frac{2\pi}{M}$ for all sectors $i, j = 1, \ldots, M$. We will refer to this special class of antennas as equal-sector antennas (ESAs) and parameterize them via the side-sector suppression a_{s} that determines the beamwidth as $\beta = 2\pi/[M\sqrt{\ln(1/a_{\mathrm{s}})}]$ [11]. In practice, antennas such as the LWA [14] that we use in our measurements (see Section VII) cannot be modeled as ESAs since the beamwidth as well as the attenuation vary for different sectors. An SBS composed of a circular antenna array, in contrast, has approximately constant α_m and β_m and can hence be modeled as an ESA.

Initially, every RX k computes so-called sector-powers from the N received samples $r_{k,m}(n)$ in sector m according to

$$\epsilon_{k,m} = \frac{1}{N}\sum_{n=0}^{N-1} \left| r_{k,m}(n) \right|^2 . \tag{2}$$

In free space, the received signal samples can be modeled as [12]

$$r_{k,m}(n) = \zeta_m(\varphi_k) s_{k,m}(n) + w_{k,m}(n) \tag{3}$$

where $s_{k,m} \sim \mathcal{CN}(0, \gamma_k)$ is the incoming signal impinging with DoA φ_k on RX k in sector m with RSS γ_k, and $w_{k,m}(n) \sim \mathcal{CN}(0, \sigma_{\mathrm{w}}^2)$ is additive noise. As shown in [12], we can then approximate the distribution of the sector-powers as $\epsilon_{k,m} \sim \mathcal{N}(\tilde{\mu}_{k,m}, \tilde{\sigma}_{k,m}^2)$ with $\tilde{\mu}_{k,m} = \mathrm{E}[\epsilon_{k,m}] = \rho_{k,m}\gamma_k + \sigma_{\mathrm{w}}^2$ and $\tilde{\sigma}_{k,m}^2 = \mathrm{var}[\epsilon_{k,m}] = \frac{1}{N}(\rho_{k,m}\gamma_k + \sigma_{\mathrm{w}}^2)^2$ where $\rho_{k,m} = [\zeta_m(\varphi_k)]^2$.

In multipath scenarios, in contrast, we use the following model for the received signal samples

$$r_{k,m}(n) = \sum_{g=1}^{G} \zeta_{k,m,g}\psi_{k,g} s_{k,m}(n) + w_{k,m}(n) \tag{4}$$

where G is the number of paths, $\zeta_{k,m,g} = \zeta_m(\varphi_{k,g})$ is the attenuation from the mth sector of the kth RX on the DoA of the gth path $\varphi_{k,g}$, and $\psi_{k,g}$ is the power scaling of the gth path. We assume $g = 1$ is the path with the greatest power (e.g., line-of-sight path), so that $\psi_{k,1} > \psi_{k,g},\ \forall\, g > 1$. We further assume path powers sum to unity, i.e., $\sum_{g=1}^{G} \psi_{k,g}^2 = 1$. Note that in (4) we assume the sample time delays among multiple paths are negligible. This assumption is valid when the signal bandwidth is significantly smaller than the channel coherence bandwidth, or all paths with delays greater than the sample period obtain small energies. More complicated multipath signal models with significant delays among paths will be included in our future work. Notice, however, that the above model anyway takes into account the different arriving angles of different multipath components. Similar to the free space scenario, we can approximate the sector-powers as $\epsilon_{k,m} \sim \mathcal{N}(\bar{\mu}_{k,m}, \bar{\sigma}_{k,m}^2)$, with $\bar{\mu}_{k,m} = \eta_{k,m}^2\gamma_k + \sigma_{\mathrm{w}}^2$ and $\bar{\sigma}_{k,m}^2 = \frac{1}{N}(\eta_{k,m}^2\gamma_k + \sigma_{\mathrm{w}}^2)^2$, where $\eta_{k,m} = \sum_{g=1}^{G} \zeta_{k,m,g}\psi_{k,g}$.

For ease of presentation and without loss of generality, we moreover make the following simplifying assumptions in this paper:

- All RXs are equipped with a similar kind of antenna.
- Sector-orientations ϑ_m, $m = 1, \ldots, M$ are the same at all RXs.
- Sectors are numbered in ascending order of their orientation, i.e., $\vartheta_m < \vartheta_{m+1}$, $m = 1, \ldots, M$.

III. Three-Stage SLS DoA Estimation

The underlying principle of TSLS DoA estimation is similar to that of our earlier proposed SLS DoA estimator. In fact, for ESAs and $L = 2$, TSLS results in the same DoA estimates as SLS. However, in contrast to SLS, TSLS DoA estimation can be based on $L > 2$ sectors. As depicted in Fig. 3, TSLS first selects a subset $\mathcal{L}_k$, $|\mathcal{L}_k| = L$ of all sectors, subsequently estimates a SP-DoA, $\hat{\varphi}_{k,ij}$, for all sector pairs (i, j), $i, j \in \mathcal{L}_k$, $i \neq j$, and finally obtains the DoA estimate, $\hat{\varphi}_k$, through weighted fusion of the SP-DoAs. The three stages of TSLS DoA estimation are discussed in detail in the following sections.

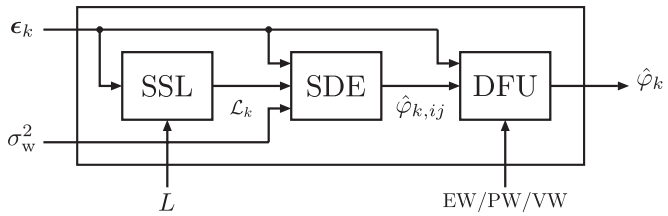

Fig. 3. The three stages of TSLS DoA estimation: sector selection (SSL), SP-DoA estimation (SDE) and DoA fusion (DFU) with the weighting methods equal weighting (EW), power weighting (PW), and variance weighting (VW).

A. Sector Selection (SSL)

The purpose of SSL is to find the subset $\mathcal{L}_k$ containing the L sectors that are best suited to extract the DoA from their respective sector-powers. Towards that end, SSL first finds the maximum adjacent sector-pair (MASP), i.e., the sector-pair $(q, q+1)$ such that $\epsilon_{k,q}\epsilon_{k,q+1} > \epsilon_{k,l}\epsilon_{k,l+1}$ for all other sector-pairs $(l, l+1)$, $l = 1, \ldots, M$, $l \neq q$. Thus, when α_m does not vary too strongly with m, $\vartheta_q < \varphi_k < \vartheta_{q+1}$ with high probability. For even L, SSL then returns the sector subset $\mathcal{L}_k = \{q - L/2 + 1, \ldots, q + L/2\}$. For odd L, SSL next estimates whether φ_k is closer to ϑ_q or ϑ_{q+1}. This is achieved by comparing $\epsilon_{k,q}$ and $\epsilon_{k,q+1}$. If $\epsilon_{k,q} > \epsilon_{k,q+1}$ then SSL estimates that $|\varphi_k - \vartheta_q| < |\varphi_k - \vartheta_{q+1}|$ and returns $\mathcal{L}_k = \{q - (L+1)/2 + 1, \ldots, q + (L-1)/2\}$. Otherwise, $\mathcal{L}_k = \{q - (L-1)/2 + 1, \ldots, q + (L+1)/2\}$ is returned. Note that for clarity we have not considered that the sector indices are circular for antennas spanning the whole 360° range, i.e., sector 1 is also adjacent to sector M. However, the extension of the above to the circular case is trivial.

We have compared this SSL method to other methods such as picking the L sectors with the L maximum sector-powers. For the ESA and LWA that we discuss in more detail in Section VI-B, we found that the above described method works best. It is important to note though that the best SSL method for one antenna type might not necessarily be the best for another antenna type. For example, if α_m varies strongly with the sectors m, then another SSL might perform better. On the other hand, if α_l is particularly small in a sector l, then sector l is not suitable for DoA estimation anyways, as the TX signal is severely attenuated in that sector.

B. Sector-Pair DoA Estimation (SDE)

In TSLS a SP-DoA is estimated for all sector-pairs (i, j), $i, j \in \mathcal{L}_k$, $i \neq j$. Towards that end, the noise-centered sector-powers (NCSP) are first calculated as

$$p_{k,i} = \epsilon_{k,i} - \sigma_{\mathrm{w}}^2. \tag{5}$$

Thereafter, NCSPs with $p_{k,i} < 0$ are discarded and the respective sectors are removed from $\mathcal{L}_k$. The SP-DoAs are then

obtained as the DoA $\hat{\varphi}_{k,ij}$ that minimizes the squared error of the ratio of NCSPs from sector i and j, i.e.,

$$\hat{\varphi}_{k,ij} = \arg\min_{\varphi} \left(\frac{p_{k,i}}{p_{k,j}} - \frac{\rho_{k,i}(\varphi)}{\rho_{k,j}(\varphi)} \right)^2. \quad (6)$$

In that way, we can estimate the DoA without estimating the RSS, which is also contained in $p_{k,m}$, $m = i, j$ but with good approximation not anymore in the ratio $p_{k,i}/p_{k,j}$. In order to obtain a closed-form solution to (6), we assume that the main beam of the antenna can be approximated through a Gaussian curve, which is possible for many practical antennas [26], [29]. This closed-form solution is different for EBS and DBS as derived in Appendix A.

1) Equal Beamwidth Sectors: The solution of (6) for EBS is straight-forward and is given by

$$\hat{\varphi}_{k,ij} = \bar{\vartheta}_{ij} + \kappa_{ij} \left(\ln \frac{p_{k,i}}{p_{k,j}} - 2 \ln \frac{\alpha_i}{\alpha_j} \right) \quad (7)$$

with $\bar{\vartheta}_{k,ij} = \frac{1}{2}(\vartheta_i + \vartheta_j)$ and $\kappa_{ij} = \frac{\beta^2}{4(\vartheta_i - \vartheta_j)}$. For the special case of $\alpha_i = \alpha_j$ we obtain the equation for classical SLS that we have already derived in [11].

2) Different Beamwidth Sectors: For DBS the minimization in (6) results in a quadratic equation and has, hence, two solutions of the form

$$\hat{\varphi}_{k,ij}^{[1/2]} = \lambda_{ij} \pm b_{ij} g(p_{k,i}, p_{k,j}) \quad (8)$$

with

$$g(\mathbf{p}) = \sqrt{(\Delta\vartheta_{ij})^2 - \Delta\beta_{ij} \ln \frac{\alpha_i}{\alpha_j} + \frac{1}{2} \Delta\beta_{ij} \ln \frac{p_{k,i}}{p_{k,j}}}, \quad (9)$$

where $\mathbf{p} = (p_{k,i}, p_{k,j})^T$, $\lambda_{ij} = \frac{\beta_i^2 \vartheta_j - \beta_j^2 \vartheta_i}{\Delta\beta_{ij}}$, $b_{ij} = \frac{\beta_i \beta_j}{\Delta\beta_{ij}}$, $\Delta\beta_{ij} = \beta_i^2 - \beta_j^2$, and $\Delta\vartheta_{ij} = \vartheta_i - \vartheta_j$. The ambiguity in (8) can be resolved by taking the NCSPs into account. For each of the solutions $\hat{\varphi}_{k,ij}^{[l]}$ $l = 1, 2$, we can estimate two RSSs as $\hat{\gamma}_{k,ij,m}^{[l]} = \frac{p_{k,m}}{\hat{\rho}_{k,ij,m}^{[l]}}$, where $m = i, j$ and $\hat{\rho}_{k,ij,m}^{[l]} = [\alpha_m \exp(-[\mathcal{M}(\hat{\varphi}_{k,ij}^{[l]} - \vartheta_m)]^2 / \beta_m^2)]^2$ is the estimated attenuation in sector m given that the DoA is $\hat{\varphi}_{k,ij}^{[l]}$. In the case $N \to \infty$, the two RSS estimates per DoA solution $\hat{\varphi}_{k,ij}^{[l]}$, $l = 1, 2$ are equal, i.e., $\hat{\gamma}_{k,ij,i}^{[l]} = \hat{\gamma}_{k,ij,j}^{[l]}$, if $\hat{\varphi}_{k,ij}^{[l]} = \varphi_k$. Therefore, we choose the solution l in (8) such as to minimize $|\hat{\gamma}_{k,ij,i}^{[l]} - \hat{\gamma}_{k,ij,j}^{[l]}|$. If $g(\mathbf{p})$ becomes imaginary, the respective SP-DoA estimate is discarded.

C. DoA Fusion (DFU)

SDE results in P SP-DoA estimates $\hat{\varphi}_{k,ij} = \varphi_k + \delta\hat{\varphi}_{k,ij}$ that have to be fused together in order to obtain the final DoA estimate. Obviously, it is desirable to give larger weight to those SP-DoA estimates that have a smaller error $\delta\hat{\varphi}_{k,ij}$. However, $\hat{\varphi}_{k,ij}$ are circular random variables such that conventional weighted averaging is not applicable. Instead, we use a weighted fusion method for circular random variables as discussed in [30]:

$$\frac{\sin \hat{\varphi}_k}{\cos \hat{\varphi}_k} = \frac{\sum w_{k,ij} \sin \hat{\varphi}_{k,ij}}{\sum w_{k,ij} \cos \hat{\varphi}_{k,ij}}, \quad (10)$$

where we denote the weights for DoA $\varphi_{k,ij}$ as $w_{k,ij}$. Geometrically, (10) can be interpreted as the summation of P vectors with magnitude $w_{k,ij}$ and angle $\hat{\varphi}_{k,ij}$ in a two-dimensional plane. The resulting vector then has an angle that is equal to the final DoA estimate $\hat{\varphi}_k$. Our simulations have shown that (10) has identical performance to conventional weighted averaging if the error $\delta\hat{\varphi}_{k,ij}$ is very small. However, for large $\delta\hat{\varphi}_{k,ij}$ (10) outperforms conventional weighted averaging significantly. Different choices for the weights $w_{k,ij}$ are discussed next.

1) Equal Weighting (EW): For equal weighting of the SP-DoAs, the weights can simply be set to $w_{k,ij}^{\mathrm{EW}} = 1$.

2) Sector-Power Weighting (PW): Based on the discussion in Section III-A, sector-powers are a good indication for the potential contribution of different sectors in DoA estimation. Consequently, an intuitive and robust weighting scheme for SP-DoA $\hat{\varphi}_{k,ij}$ is the product of NCSPs i and j

$$w_{k,ij}^{\mathrm{PW}} = p_{k,i} p_{k,j}. \quad (11)$$

3) Variance Weighting (VW): If the variance $\sigma_{ij}^2 = \mathrm{var}[\delta\hat{\varphi}_{k,ij}]$ of individual SP-DoA errors is known, a weighting scheme $w_{k,ij} = 1/\sigma_{ij}^2$ can be applied. However, in practice the knowledge of σ_{ij}^2 is not a realistic assumption. In Section IV-A we derive an approximation $v_{k,ij}^{(1)} \approx \sigma_{ij}^2$ of the SP-DoA error variance in free space. This variance can be estimated as $\hat{v}_{k,ij}^{(1)}$, simply by approximating the $\mu_{k,i}$ that is contained in (19) via $a_{k,i}$ as $p_{k,i}$. Thus, a variance-based weighting scheme can be achieved by setting

$$w_{k,ij}^{\mathrm{VW}} = \left(\hat{v}_{k,ij}^{(1)} \right)^{-1}. \quad (12)$$

D. Validity Check

In particular for low SNR it is possible that $p_{k,i} < 0 \ \forall\, i = 1, \ldots, M$ or that all SP-DoAs are discarded, as discussed in Section III-B2. Then $P = 0$ and DFU stage cannot be executed. In that case, TSLS estimates the DoA using the modified maxE estimator introduced in [31].

IV. Analytical Models for the Error of SP-DoA Estimation

In this section we derive analytical models for the error of the SP-DoA estimates obtained in SDE. Towards that end, we first notice that $p_{k,m}$ is distributed as $p_{k,m} \sim \mathcal{N}(\mu_{k,m}, \sigma_{k,m}^2)$ with $\mu_{k,m} = \mathrm{E}[p_{k,m}] = \rho_{k,m}\gamma_k$ and $\sigma_{k,m}^2 = \mathrm{var}[p_{k,m}] = \frac{1}{N}(\rho_{k,m}\gamma_k + \sigma_{\mathrm{w}}^2)^2$. We then assume that $\sigma_{k,m}^2 \ll \mu_{k,m}$, which holds for sufficiently high SNR and a moderate to large number of samples. Given this assumption, we can approximate the SP-DoA estimate $\hat{\varphi}_{k,ij}$ through its n-th order Taylor series expansion developed around the means $p_{k,i} = \mu_{k,i}$ and $p_{k,j} = \mu_{k,j}$. In our derivation we will be using the following lemma:

Lemma 1: Given an $L \times 1$ random vector $\mathbf{X} \sim \mathcal{N}(\boldsymbol{\mu}, \mathbf{Q})$ with mean vector $\boldsymbol{\mu} = \mathrm{E}[\mathbf{X}]$ and diagonal covariance $\mathbf{Q} = \mathrm{E}[(\mathbf{X} - \boldsymbol{\mu})(\mathbf{X} - \boldsymbol{\mu})^T] = \mathrm{diag}[\sigma_1^2, \ldots, \sigma_L^2]$, and the random variable $Y = f(\mathbf{X})$, where $f : \mathbb{R}^{L \times 1} \to \mathbb{R}$. Denote $Y^{(n)}(\boldsymbol{\mu})$ as the n-th order Taylor series of Y around $\boldsymbol{\mu}$, the gradient of Y as $\mathbf{j} = \frac{\partial f}{\partial \mathbf{X}_1}\mathbf{e}_1 + \ldots + \frac{\partial f}{\partial \mathbf{X}_L}\mathbf{e}_L$ and the Hessian matrix of Y as $\mathbf{H}$. Then,

we obtain the expected values of the first and second order Taylor series of Y developed around its mean as

$$\mathrm{E}\left[Y^{(1)}(\boldsymbol{\mu})\right] = f(\boldsymbol{\mu}) \tag{13}$$

$$\mathrm{E}\left[Y^{(2)}(\boldsymbol{\mu})\right] = f(\boldsymbol{\mu}) + \frac{1}{2}\mathrm{trace}\left\{\mathbf{H}(\boldsymbol{\mu})\mathbf{Q}\right\} \tag{14}$$

and the respective variances as

$$\mathrm{var}\left[Y^{(1)}(\boldsymbol{\mu})\right] = \sum_l \mathbf{j}_l^2(\boldsymbol{\mu})\sigma_l^2 \tag{15}$$

$$\mathrm{var}\left[Y^{(2)}(\boldsymbol{\mu})\right] = \sum_l \mathbf{j}_l^2(\boldsymbol{\mu})\sigma_l^2 + \frac{1}{2}\mathrm{trace}\left\{(\mathbf{H}(\boldsymbol{\mu})\mathbf{Q})^2\right\}. \tag{16}$$

A detailed derivation of this lemma can be found in Appendix B.

A. Free Space Propagation

The approximations for bias and variance of SP-DoA estimation that we present in the following are derived for DBS, i.e., the SP-DoA estimator (8). Following similar steps, we can also obtain bias and variance approximations for EBS, i.e., the SP-DoA estimator (7). However, the resulting EBS approximations are in fact equal to the DBSs approximations when noting that $\beta_i = \beta_j$ and therefore replacing $\Delta\beta_{ij} = 0$ in (17)–(20) in the EBS case.

For the derivations, we first assume that the SP-DoA estimated in the SDE stage is the correct one out of the two possibilities in (8), which is a very reasonable assumption as discussed later in Section VI-B. Next, we approximate the SP-DoA through its n-th order Taylor series as $\hat{\varphi}_{k,ij} \approx \hat{\varphi}_{k,ij}^{(n)}$. Using Lemma 1 and following the derivations in Appendix C, we then obtain an approximation of the bias $\mathrm{E}[\hat{\varphi}_{k,ij}] - \varphi_k \approx b_{k,ij}^{(n)} = \mathrm{E}[\hat{\varphi}_{k,ij}^{(n)}] - \varphi_k$ through first and second-order Taylor series as

$$b_{k,ij}^{(1)} = 0 \tag{17}$$

$$b_{k,ij}^{(2)} = \pm\frac{\beta_i\beta_j}{8g(\boldsymbol{\mu})}\left[a_{k,j} - a_{k,i} - \frac{\Delta\beta_{ij}}{4g^2(\boldsymbol{\mu})}(a_{k,i} + a_{k,j})\right] \tag{18}$$

where $a_{k,m} = \frac{1}{N}\left(\mathrm{SNR}_{k,m}^{-1} + 1\right)^2$, $\mathrm{SNR}_{k,m} = \frac{\mu_{k,m}}{\sigma_w^2} = \rho_{k,m}\mathrm{SNR}_k$. Using the same approach, we can also approximate the variance of the SP-DoA estimation error through its n-th order Taylor series, i.e., $\mathrm{var}[\hat{\varphi}_{k,ij}] \approx v_{k,ij}^{(n)} = \mathrm{var}\left[\hat{\varphi}_{k,ij}^{(n)}\right]$. For the first and second order Taylor approximations, the variances are then equal to

$$v_{k,ij}^{(1)} = \frac{\beta_i^2\beta_j^2}{16\left[g(\boldsymbol{\mu})\right]^2}(a_{k,i} + a_{k,j}) \tag{19}$$

$$v_{k,ij}^{(2)} = \frac{\beta_i^2\beta_j^2}{16g^2(\boldsymbol{\mu})}\left[a_{k,i} + a_{k,j} + \frac{1}{2}\left(a_{k,i}^2 + a_{k,j}^2\right) + \frac{\Delta\beta_{ij}}{4g^2(\boldsymbol{\mu})}\left(a_{k,i}^2 - a_{k,j}^2\right) + \frac{\Delta^2\beta_{ij}}{32g^4(\boldsymbol{\mu})}(a_{k,i} + a_{k,j})^2\right]. \tag{20}$$

The derivation of (19)–(20) is again based on Lemma 1 with the details given in Appendix C.

B. Multipath Propagation

In this subsection we present the bias and variance of SP-DoA estimation when multipath is considered. We present only results for EBS due to their mathematical conciseness. It is straightforward to extend the derivation to DBS. Following Lemma 1, the bias of the SP-DoA using first and second order Taylor approximations are given by

$$\bar{b}_{k,ij}^{(1)} = \bar{\vartheta}_{k,ij} + \kappa_{ij}\left(2\ln\frac{\eta_{k,i}}{\eta_{k,j}} - \ln\frac{\alpha_i}{\alpha_j}\right) - \varphi_{k,1} \tag{21}$$

$$\bar{b}_{k,ij}^{(2)} = \bar{b}_{k,ij}^{(1)} - \frac{1}{2}\left(\frac{\kappa_{ij}\bar{\sigma}_{k,i}^2}{\gamma_k^2\eta_{k,i}^4} - \frac{\kappa_{ij}\bar{\sigma}_{k,j}^2}{\gamma_k^2\eta_{k,j}^4}\right), \tag{22}$$

respectively, where $\varphi_{k,1}$ is the DoA of the strongest path, i.e., the "true" DoA. The variances are equal to

$$\bar{v}_{k,ij}^{(1)} = \frac{\kappa_{ij}^2\bar{\sigma}_{k,i}^2}{\gamma_k^2\eta_{k,i}^4} + \frac{\kappa_{ij}^2\bar{\sigma}_{k,j}^2}{\gamma_k^2\eta_{k,j}^4} \tag{23}$$

$$\bar{v}_{k,ij}^{(2)} = \bar{v}_{k,ij}^{(1)} + \frac{1}{2}\left(\frac{\kappa_{ij}^2\bar{\sigma}_{k,i}^4}{\gamma_k^4\eta_{k,i}^8} + \frac{\kappa_{ij}^2\bar{\sigma}_{k,j}^4}{\gamma_k^4\eta_{k,j}^8}\right). \tag{24}$$

The derivations of (21)–(24) are very similar to Section IV-A and Appendix C, and are thus omitted due to space limitation.

V. Localization

DoA estimates $\hat{\varphi}_k$ from individual sensors $k, k = 1, \ldots, K$, are fused together into a location estimate using a modified version of the Stansfield algorithm [11]. The original Stansfield algorithm was proposed in [28] as an approximation to the maximum likelihood estimator. Its location estimate $\hat{\boldsymbol{\ell}} = (\hat{x}_\mathrm{P}, \hat{y}_\mathrm{P})^T$ is obtained as

$$\hat{\boldsymbol{\ell}} = (\mathbf{A}^T\mathbf{W}\mathbf{A})^{-1}\mathbf{A}^T\mathbf{W}\mathbf{b}, \tag{25}$$

with

$$\mathbf{A} = \begin{bmatrix} \sin(\hat{\varphi}_1) & -\cos(\hat{\varphi}_1) \\ \vdots & \vdots \\ \sin(\hat{\varphi}_K) & -\cos(\hat{\varphi}_K) \end{bmatrix}, \tag{26}$$

$$\mathbf{b} = \begin{bmatrix} x_1\sin(\hat{\varphi}_1) - y_1\cos(\hat{\varphi}_1) \\ \vdots \\ x_K\sin(\hat{\varphi}_K) - y_K\cos(\hat{\varphi}_K) \end{bmatrix} \tag{27}$$

and a weighting matrix $\mathbf{W}$. In the original Stansfield algorithm, the weighting matrix is dependent on both the individual TX-RX distances as well as the quality of the DoA estimates. In practice this information is not available for the DoA fusion. Therefore, we use the modified version [11] where the contribution of each sensor k is weighted with an estimate of the sensor's RSS, $\hat{\gamma}_k$. This results in a diagonal weighting matrix $\mathbf{W} = \mathrm{diag}(\hat{\gamma}_1, \hat{\gamma}_2, \ldots, \hat{\gamma}_K)$.

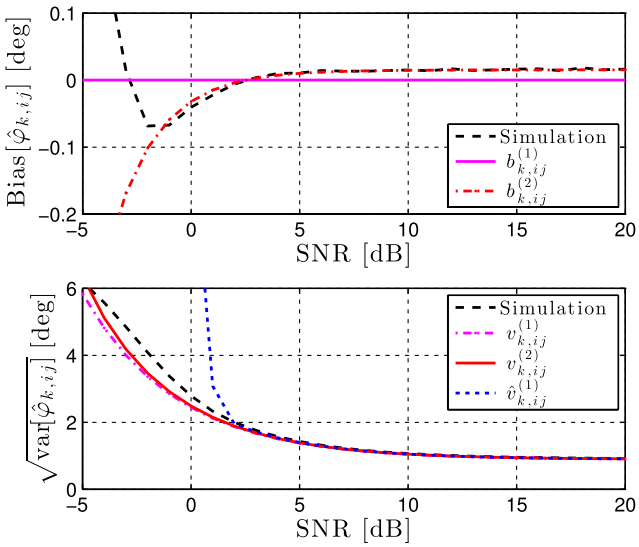

Fig. 4. Analytical and empirical bias and standard deviation of sector-pair DoA estimation in free space.

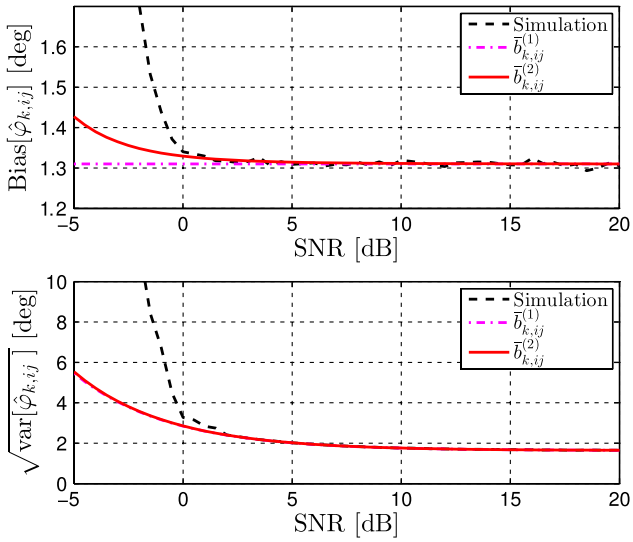

Fig. 5. Analytical and empirical bias and standard deviation of sector-pair DoA estimation with multipath.

VI. Numerical Evaluations and Analysis

As the following presentation builds heavily on previously-defined abbreviations, the reader may refer to Table I for a summary of the most commonly used ones.

A. Error of SP-DoA Estimation

We analyze the error of SP-DoA estimation in free space using two sectors with $\alpha_i = 1$, $\alpha_j = 0.9$, $\beta_i = 1/2$ rad, $\beta_j = 1/3$ rad, $\vartheta_i = 0°$, $\vartheta_j = 20°$ and an incoming signal DoA of $\varphi_k = 10°$. These numbers reflect a realistic example scenario, though any other numerical values could be used as well. Fig. 4 depicts the bias and standard deviation of the SP-DoA estimator proposed in Section III-B. The simulated curves are obtained empirically over 10^6 realizations per SNR-step while the analytical curves are obtained by calculating the first and second order Taylor approximation models derived in Section IV-A.

We first notice that the SP-DoA estimates are slightly biased, even for large SNR. This bias is nicely described by the 2nd-order Taylor approximation from SNR ≈ -2 dB onwards. The 1st-order approximation, in contrast, fails to model the bias adequately. However, the sectors considered in here are DBS. For EBS, we have $\beta_i = \beta_j$ in (18) such that $b^{(2)}_{k,ij} \to 0$ for SNR $\to \infty$ since $a_{k,i} \to a_{k,j} \to \frac{1}{N}$. Hence, SP-DoA estimation with EBS is asymptotically unbiased for large SNR as we have confirmed already for SLS in [12], [13].

With respect to the variance, both 1st- and 2nd-order Taylor approximations model the behavior very well for low to high SNR. Only for very low SNR < 0 dB, we observe that $v^{(2)}_{k,ij}$ approximates the variance slightly more accurately. For comparison, we have also included the estimate of the 1st-order Taylor variance approximation, $\hat{v}^{(1)}_{k,ij}$ that is calculated according to the discussion in Section III-C3. This estimate is very accurate for SNR > 2 dB. However, for SNRs below 2 dB, the slope of the variance estimates is very steep, resulting in overly pessimistic estimates in the low SNR range. This is a consequence of $a_{k,m}$, $m = i, j$ in the estimation of (19) behaving proportional to $1/p^2_{k,m}$ for low SNRs. Since $p_{k,m}$ is symmetrically distributed around its mean, $a_{k,m}$ is hence on average estimated larger than it actually is. For TSLS DoA estimation this means that a DFU weighting with an estimated 2nd order Taylor approximation variance (20) cannot be beneficial, as $v^{(2)}_{k,ij}$ is only slightly more accurate than $v^{(1)}_{k,ij}$ for SNRs that are anyways already too low to estimate the variance properly.

We next proceed to analyze the error of SP-DoA estimation in multipath scenarios, using two sectors with $\alpha_i = 1, \alpha_j = 0.9$, $\vartheta_i = 0°$, $\vartheta_j = 20°$. Since our results for multipath in Section IV-B are for EBS, we calculate the common β of the two sectors from a setting of $M = 6$ and $a_s = 0.4$. We include two paths in our simulations: a line-of-sight path with power scaling $\psi^2_{k,1} = 0.9$ and DoA $\varphi_{k,1} = 10°$, and a reflected path with power scaling $\psi^2_{k,2} = 0.1$ and DoA $\varphi_{k,2} = 15°$. Similarly to our example of free space propagation, these numbers reflect a realistic example scenario. Naturally, other numerical values could be used for multipath propagation as well. Our results of simulated bias and standard deviation, as well as theoretical results using the 1st- and 2nd-order Taylor approximations derived in Section IV-B, are shown in Fig. 5.

We observe that the SP-DoA estimates are more strongly biased in a multipath scenario than in free space, as the bias increased from 0.02° in Fig. 4 to 1.3° in Fig. 5 for SNR greater than 5 dB. The bias increase is primarily because of the reflected path that is 5° away from the main path. Both theoretical bias using the 1st- and 2nd-order Taylor approximations match the empirical simulations for SNR greater than 0 dB. The gap between theoretical and simulation results is smaller for the 2nd-order curve compared to the 1st-order curve. The standard deviation of the SP-DoA estimations under multipath is also greatly increased compared with the free space scenario, e.g., for 10 dB the standard deviation is 1° in free space and 2° with multipath. Theoretical results using 1st- and 2nd-order Taylor

approximations behave similarly, i.e., they match simulations accurately for SNR greater than 0 dB.

Note that the root-mean squared error (RMSE) of SP-DoA estimation will increase in multipath scenarios due to the increased bias and variance. This fact will further affect the TSLS DoA estimation and transmitter localization performance. However, due to space limitation, the following sections only contain simulation results without multipath. In Section VII, the impact of severe multipath on DoA estimation and localization accuracy will be further discussed and elaborated with practical RF measurements.

B. TSLS DoA Estimation Performance

The performance of TSLS DoA estimation is evaluated next using two different antenna models. On the one hand, we study the performance using an ESA with $M = 6$ sectors, each with a radiation pattern as in (1) and $a_s = 0.4$. On the other hand, we consider a model of an actual LWA that we use in the practical measurements in Section VII. The LWA is modeled using the radiation patterns according to (1) with the parameters $\alpha_m = \hat{\alpha}_m$, $\beta_m = \hat{\beta}_m$ and $\vartheta_m = \hat{\vartheta}_m$ shown in Table III. These parameters were obtained from a least-squares (LS) fit of the actual radiation pattern as discussed in more detail in Section VII-B. In total, the LWA has $M = 12$ sectors with orientations ranging from roughly $-50°$ to $50°$, making the antenna suitable for DoAs from around $-60°$ to $60°$. In contrast, the ESA covers the entire angular range from $-180°$ to $180°$. However, with respect to TSLS DoA estimation, the main difference between the two models is that the ESA consists entirely of EBS, while the LWA model has only DBS. Therefore, TSLS is run with the SP-DoA estimation as described in Section III-B1 for the former, while the latter uses SP-DoA estimation as discussed in Section III-B2. It is assumed that the DoA is uniformly distributed over the whole angular coverage area of the antennas. We emulate this distribution via 100 equidistant steps in the interval $\varphi_k \in \left[0; \frac{180°}{M}\right)$ for the ESA [12] and 120 equidistant steps in the interval $\varphi_k \in [-60°; 60°)$ for the LWA model. For each DoA-step we then simulate 2000 realizations, and average over the results at each step in order to obtain the RMSE. In the following, we will be using different configurations of TSLS, such as TSLS+EW. Please refer to Fig. 3 for an overview of the configurations and to Section III for detailed descriptions.

Fig. 6 depicts the RMSE of DoA estimation as a function of the SNR when using the ESA. For reference, we have also included the CRB on DoA estimation with sectorized antennas [12], along with the SLS DoA estimator [12]. For TSLS, we have determined that $L = 3$ provides the best performance for moderate to high SNRs in separate simulations that are not explicitly shown due to space limitations. Note that this value is specific to the antenna and in particular its beamwidth as will be discussed later in this section. From the results in [12] it can be concluded that SLS is not making efficient use of high SNRs. In contrast, TSLS with EW in the DFU stage is approaching the CRB for large SNR ≈ 20 dB. However, the performance of TSLS+EW degrades rapidly for lower SNRs such that SLS outperforms TSLS+EW already for SNR ≈ 12 dB. The

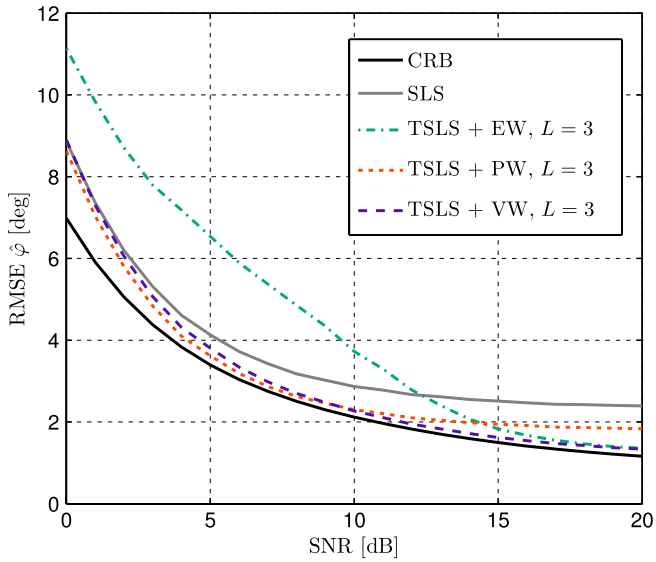

Fig. 6. DoA estimation performance with equal-sector antenna and different algorithms. Parameters: $a_s = 0.4$, $M = 6$, and $N = 100$.

combination of TSLS and PW performs best of all algorithms for the low SNR region, while its performance saturates at a higher RMSE than the CRB and the other TSLS configurations, starting from SNR ≈ 10 dB. Nevertheless, it outperforms SLS for all SNRs. The overall best performance is achieved with TSLS+VW. For low SNR, TSLS+VW behaves like SLS and performs therefore only slightly worse than TSLS+PW. This is explained by the earlier made observation that the variance is estimated much larger than it actually is when the sector $\text{SNR}_{k,m}$ is low. In the DFU stage and for overall low SNR this therefore leads to an implicit exclusion of all SP-DoAs other than the one used in SLS. For high SNR, on the other hand, TSLS+VW performs like TSLS+EW. This, in turn, is explained by the variance of the SP-DoA estimates that become independent of the sector for very large SNRs and ESAs since $a_{k,m} \to \frac{1}{N}$ for SNR $\to \infty$ in (19).

The performance of the LWA model as a function of the SNR is shown in Fig. 7. Although the CRB was only discussed for ESAs in [12], it was derived in a generic format such that it is also applicable for our LWA model. Therefore, we have included the CRB as a reference also in this figure. Besides the sector parameters, α_m and β_m varying for different sectors m, the LWA model also has a much bigger overlap between the sectors than the ESA. As an example, the sectors 3 and 4 (Table III) have $\alpha_4 \approx \alpha_3 = 1$ and $\Delta\vartheta_{43} \approx 12°$. With these parameters an ESA would have $M = 30$ sectors, resulting in $\beta \approx 0.22$ rad if we assume the same side-sector suppression $a_s = 0.4$ as for the above described ESA. The LWA antenna, in contrast, has an almost 8-fold larger beamwidth in the sectors 3 and 4. Compared to the ESA, much more sectors of the LWA therefore receive the TX signal at a high SNR. This, in turn, implies that L, i.e., the number of sectors used for SP-DoA estimation, should be increased for the LWA. We have found that parameterizing TSLS with $L = 11$ results in the overall best performance. However, this is not the case over the whole SNR range. Using, e.g., only $L = 4$ sectors, yields a bit better

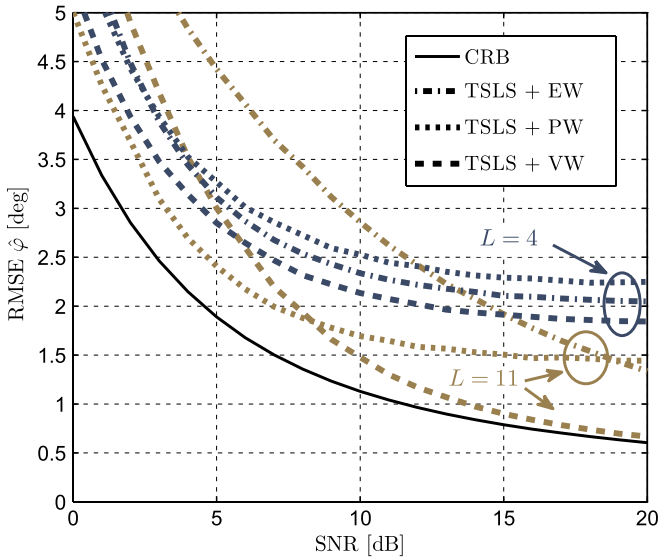

Fig. 7. DoA estimation performance with leaky-wave antenna approximated by Gaussian radiation pattern (1). Parameters: $M = 12$, $N = 100$, and antenna parameters in Table III.

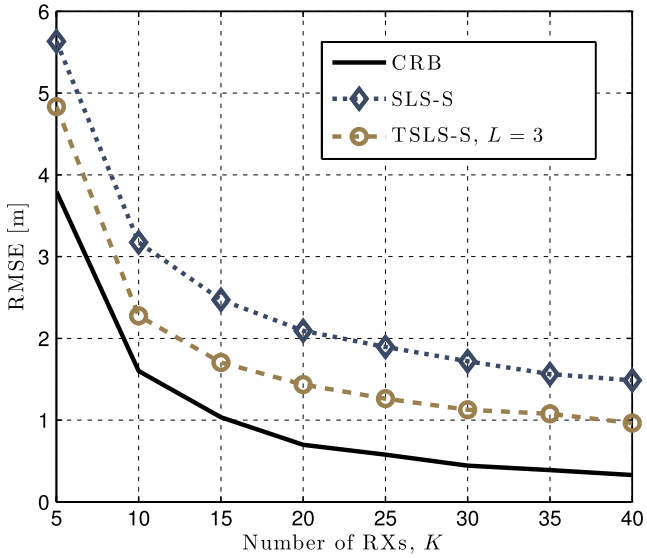

Fig. 8. Localization performance with an equal-sector antenna and a uniform distribution of RXs. Parameters: $a_s = 0.4$, $M = 6$, and $N = 100$.

performance for low SNRs if EW or VW is used in the DFU stage of TSLS. When using PW, on the other hand, it seems that the performance is best with $L = 11$ sectors for all SNRs. Otherwise, the behavior of TSLS and its DFU configurations is very similar to what we have observed already for the ESA. Most notably, TSLS+VW approaches the CRB for high SNR also for LWAs.

The SP-DoA estimator (8) yields two solutions. To verify that our selection mechanism described in Section III-B2 works properly, we have run the same simulations with the actual DoA as an input to TSLS. Out of the two possible solutions in (8), this TSLS test version then picks the one that is closer to the actual DoA. Naturally, this test version yields better performance than the practical implementation. However, the increase in performance is only marginal. Therefore, we can conclude that the selection mechanism based on the RSS works well. For clarity of presentation, we have not included these test curves in Fig. 7.

C. Localization Performance

In this section, we evaluate the performance of localization with TSLS+VW DoA estimation and subsequent Stansfield fusion (TSLS-S). For comparison, we also include the combination of SLS and Stansfield (SLS-S) as well as the CRB on non-cooperative TX localization using sectorized antennas [29]. In our simulation, we assume that the RXs are uniformly distributed on a circle with radius $R = 150$ m centered around the TX. However, no RX is placed in a protective inner circle with radius $R_0 = 5$ m. The TX transmit power is $P_T = 20$ dBm, while the measurement noise power at the RXs is $\sigma_w^2 = -70$ dBm. For the propagation, we assume a log-distance path loss model with path loss exponent $\alpha = 4$. Overall, these settings result in an average $\overline{\text{SNR}} = 10\log_{10}\left(\frac{2}{\alpha-2}\frac{P_T}{\sigma_w^2}\frac{R_0^{2-\alpha}-R^{2-\alpha}}{R^2-R_0^2}\right) = 33$ dB. The TX signal is modeled as bandlimited Gaussian with a bandwidth $B = 20$ MHz and without oversampling at the RXs. This leads to a correlation of sector-powers at different RXs that we have derived in detail in [29]. As we have seen in Section VI-B, the behavior of the ESA and the LWA in TSLS DoA estimation is qualitatively similar. To keep the simulations simple, we therefore assume that all RXs are equipped with an ESA, parameterized as in Section VI-B. In the simulations we obtain the RSS estimates for weighting in the modified Stansfield algorithm using the principle discussed in Section III-B2. Based on the sector-powers of the MASP and the estimated DoA at every RX k, we obtain two RSS estimates $\hat{\gamma}_{k,i}$ and $\hat{\gamma}_{k,j}$, and estimate the final RSS as $\hat{\gamma}_k = \frac{1}{2}(\hat{\gamma}_{k,i} + \hat{\gamma}_{k,j})$.

Fig. 8 depicts the RMSE of location estimation as a function of the number of RXs, K. Overall, the biggest gain in performance for increasing K is achieved for $K < 20$ RXs as reflected by the CRB as well as the algorithms. When estimating the DoA with TSLS instead of SLS, we observe a localization performance improvement of 0.5–0.8 m. This is mainly explained by the fact that the modified Stansfield algorithm is dominated by RXs with a large SNRs as we have concluded in [13]. Since TSLS is outperforming SLS in particular for moderate to large SNR, we consequently also observe a strong localization performance improvement. Nevertheless, TSLS-S is not able to approach the CRB. In this context it is, however, important to note that the CRB in [29] is derived for a more general case where the TX location is estimated directly from the *KM* sector-powers in (2). In SLS-S/TSLS-S, on the other hand, we first estimate K DoAs from the *KM* sector-powers and only thereafter we estimate the location using the DoA estimates. As we have already suggested in [29], this intermediate step might deteriorate the performance and hence it might be impossible for algorithms such as TSLS-S to exactly reach the CRB.

D. Performance and Complexity in Comparison to Related Algorithms

In this section, we compare the proposed TSLS algorithm to related works. First, we quantify the complexity of the

TABLE II
PROPOSED DoA ESTIMATOR IN COMPARISON TO OTHER ALGORITHMS

Algorithm	Complexity per DoA estimate (in basic operations)	RMSE DoA (SNR = 20 dB)	RMSE loc. ($K = 20$)
maxE [11], [22], [25]	1194 ADD +1206 MUL	17.3°	12 m
SLS [12]	1198 ADD +1213 MUL +2 LUT	2.4°	2.1 m
TSLS + VW, $L = 3$	1213 ADD +1234 MUL +10 LUT	1.3°	1.4 m

proposed TSLS DoA estimation in terms of the number of basic operations. As such, we define additions/subtractions and multiplications/divisions and refer to them as ADD and MUL, respectively. In addition to such basic operations, SLS [12] as well as TSLS rely on some standard functions that cannot be expressed directly in terms of the basic operations. For fast processing in a digital signal processor these standard functions could be implemented in form of a look-up table, which makes them neglectable in the overall processing time. Nevertheless, we include them in our considerations and refer to the natural logarithm as LOG, the exponential function as EXP, the square-root as SQR, sine/cosine as SIN/COS and finally as ATAN2 to the function that calculates the final DoA estimate from the left side of (10), which is often referred to as the *atan2* function in the literature.

Obviously, the maxE algorithm [11], [22], [25] that estimates the DoA as the sector with the maximum power has the lowest complexity since it only calculates the sector-powers according to (2) and finds the smallest of those sector-powers. The sector-power calculation is in fact also part of SLS as well as TSLS and has a complexity of $M(2N-1)\text{ADD} + M(2N+1)\text{MUL}$. Next, we derive the complexity of TSLS and obtain the complexity of SLS [12] as a by-product by setting $L = 2$ and not counting the DFU stage. In the derivation, we assume an implementation of TSLS that relies on pre-calculated values as much as possible. In (7), as an example, $\bar{\vartheta}_{ij}$, κ_{ij} and $2\ln\frac{\alpha_i}{\alpha_j}$ depend only on the approximation of the radiation pattern and can therefore be loaded as constants during runtime. Overall, this approach is very feasible for a practically reasonable number of sectors and avoids lots of computations. In the SSL stage we compute M products of sector-powers and find the maximum of those M products. The latter is comparable to finding the maximum of the M sector-powers in maxE, which we do not include in our complexity analysis since the compare operation is normally neglectable in comparison to ADD and MUL. The complexity in the SSL stage is thus equal to MMUL. In the SDE stage, we then calculate metrics $\tilde{p}_{k,i} = \ln p_{k,i},\ \forall\, i \in \mathcal{L}_k$ with complexity $L(\text{ADD} + \text{LOG})$. Thereafter, the calculation of $\ln\frac{p_{k,i}}{p_{k,j}}$ in (7) and (8) is reduced to a single subtraction. Let us now define N_{SP} as the number of sector-pairs used in the SDE stage, for which it holds that $N_{\text{SP}} \leq \binom{L}{2}$. For EBS we then obtain an overall complexity in the SDE stage equal to $(2N_{\text{SP}} + L)\text{ADD} + N_{\text{SP}}\text{MUL} + L\text{LOG}[+N_{\text{SP}}\text{ADD}]$, where the square brackets indicate operations that are only needed for antennas, where $\alpha_i \neq \alpha_j, i, j = 1, \ldots, M$. And for DBS we obtain an overall complexity of $(10N_{\text{SP}} + L)\text{ADD} + 17N_{\text{SP}}\text{MUL} + N_{\text{SP}}\text{SQR} + 4N_{\text{SP}}\text{EXP} + L\text{LOG}$ in the SDE stage. Finally, the DFU stage has a complexity of $2(N_{\text{SP}} - 1)\text{ADD} + \text{MUL} + N_{\text{SP}}(\text{COS} + \text{SIN}) + \text{AT2}$, with an additional complexity of $3N_{\text{SP}}\text{MUL}$ and $(N_{\text{SP}} + L)\text{ADD} + (4N_{\text{SP}} + 2L)\text{MUL}$ for PW and VW, respectively.

The complexity and DoA estimation performance as well as localization performance of TSLS in comparison to maxE and SLS can be found in Table II. Since SLS and maxE are estimators targeted at ESAs, we use an ESA as described in Section VI-B as the sectorized antenna, along with simulation setups as described in Section VI-B and Section VI-C for DoA estimation and localization, respectively. For simplicity, we do not separate between the aforementioned standard functions in the complexity metric. Instead, we count a call to one of the standard function as a call to a look-up table (LUT). Based on the results in Table II, we conclude that the proposed estimator has the best performance of all three, while its additional complexity is very low and mainly due to calls to standard functions, which could be handled with LUTs for fast processing.

VII. PRACTICAL RF MEASUREMENTS

A. Measurement Setup

The practical performance of the proposed TSLS DoA estimation with subsequent Stansfield localization was evaluated with the help of an extensive indoor measurement campaign at the 2.4 GHz ISM band, carried out at Drexel University. In our measurements, we used LWAs as an example of a sectorized antenna. However, other sectorized antennas such as antenna arrays with a single front-end [17], [18] would also have been a good alternative. During the measurements, several uncontrolled WiFi hotspots in the surroundings were active, causing substantial in-band interference. In addition, passers-by generated spatial and temporal variations in the measurement conditions. Both these aspects imply that the measurement environment was far from ideal, thus enhancing further the practical impact of the measurements.

As illustrated in Fig. 9, we placed a TX at three different locations and measured the signal at six RXs. The TX and RX locations were selected such that the performance could be tested in different challenging estimation scenarios. The RX antennas were oriented in such a way that they can hear the TXs within their directivity ranges in most of the cases.

Each transceiver consisted of a software defined radio platform, called Wireless Open-Access Research Platform (WARP) v3 [32]. Each WARP board was connected to its own antenna(s) and to a centralized controlling system. The TXs were equipped with omni-directional antennas whereas each RX had a single two-port LWA [21] with two antenna ports enabling simultaneous measurements in two sectors. The composite right/left-handed (CRLH) LWAs [14] were tuned to operate within the

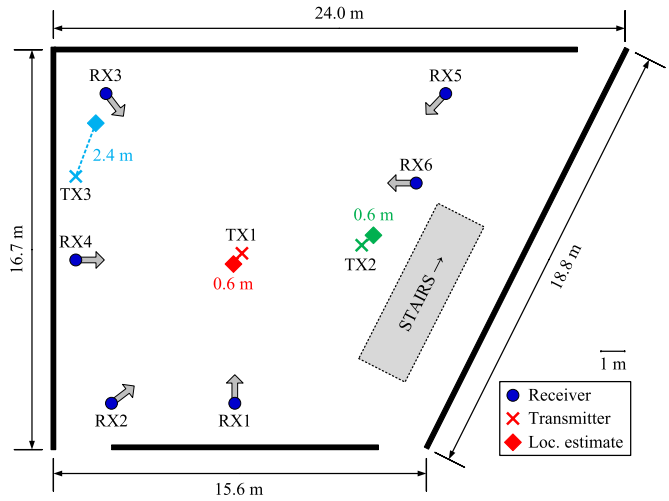

Fig. 9. Illustration of the measurement setup and the localization capabilities of the proposed algorithms in a lobby at Drexel University.

entire 2.4 GHz WiFi band. The physical size of the antenna is 156 mm × 38 mm and the antenna consists of a cascade of 12 metamaterial unit cells for obtaining good directivity and a small size simultaneously. The main beam of the antenna can be steered from broadside to backward and forward direction by changing two control voltages. Due to the practically symmetric antenna structure, antenna ports have symmetric radiation properties with respect to the broadside direction. As a trade-off between estimation complexity and estimation accuracy, we have used 6 control voltage values for a total of 12 antenna sectors.

The system was operating with a 20 MHz channel bandwidth and a carrier frequency of 2.462 GHz. This combination is heavily overlapping with the WiFi channel no. 11 which was measured to have active traffic during the measurements, acting as direct cochannel interference. The TX power was set to +15 dBm and since our algorithms rely on the received signal powers, automatic gain controls (RF and baseband) were deactivated in the RXs and the gains were set to constant values. As a practical example, we used orthogonal frequency division multiplexing (OFDM) waveforms. Only one of the transmission links, i.e., TX-RX antenna pair, was active at a time and thus we needed to ensure fairness between different transmission links by transmitting the same data over all links. Note that realistically all RXs could receive the same transmitted data only propagated through different channels. Therefore, the measurement arrangement matches the real world scenario well. For testing each link, we transmitted in total 300 packets, each containing 5420 binary phase shift keying (BPSK) symbols. Finally, for each antenna sector, we calculated the received signal power from the baseband signal snapshots by averaging over the powers of all received packets observed through the considered sector. These sector powers are then processed further using the proposed algorithms, as described in the previous sections.

B. Localization System Settings

The TSLS DoA estimator requires an approximation $\hat{\rho}_m(\varphi) = [\hat{\zeta}_m(\varphi)]^2$ of the antenna's main beam through a Gaussian curve

TABLE III
LS FIT FOR LEAKY-WAVE ANTENNA. THE LWA HAS SYMMETRIC SECTORS AROUND 0°. THEREFORE, THIS TABLE DEPICTS ONLY 6 OUT OF THE 12 SECTORS. FURTHERMORE, WE HAVE NORMALIZED THE ATTENUATION TO $\alpha_m \leq 1$, $\max(\alpha_m) = 1$, $m = 1, \ldots, M$

Sector	1	2	3	4	5	6
$\hat{\alpha}_m$	0.77	0.90	1.00	0.98	0.93	0.92
$\hat{\beta}_m$ [rad]	0.64	0.61	0.62	0.58	0.52	0.53
$\hat{\theta}_m$ [deg]	-47.9	-40.6	-29.0	-17.6	-9.5	-1.5

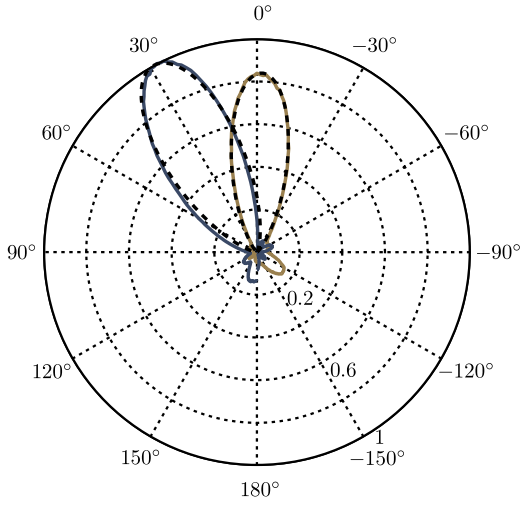

Fig. 10. Radiation pattern for two sectors (solid lines) of the leaky-wave antenna [14] used in our measurements. The main beams are well approximated by a Gaussian curve (dotted lines).

(1) in all sectors m, $m = 1, \ldots, M$. In order to obtain the approximation, we first measured the LWA's radiation pattern in each sector m as $\tilde{\rho}_m(k\Delta\varphi) = [\tilde{\zeta}_m(k\Delta\varphi)]^2$, $k = 1, \ldots, 360$ with a step-size $\Delta\varphi = 1°$. We then found an approximation through a LS fit of (1) to $\tilde{\rho}_m(k\Delta\varphi)$. However, only the main beam of the antenna can be well approximated through (1). More importantly, due to the SSL process TSLS will make use of the approximated radiation patterns only around the main beam. In order to obtain a good approximation, the LS fit was consequently calculated only around $\tilde{\vartheta}_m = \mu\Delta\varphi$, $\mu = \arg\max_k \tilde{\rho}_m(k\Delta\varphi)$, i.e., the initial estimate for the orientation of the main beam in sector m. We used an interval of $\Omega = 20°$ on both sides of $\tilde{\vartheta}_m$ and obtain $\hat{\rho}_m$ with the parameters $\hat{\alpha}_m$, $\hat{\beta}_m$ and $\hat{\vartheta}_m$ that minimize $\sum_{k=-\Omega/\Delta\varphi}^{\Omega/\Delta\varphi}[\rho_m(\tilde{\vartheta}_m + k\Delta\varphi) - \tilde{\rho}_m(\tilde{\vartheta}_m + k\Delta\varphi)]^2$. For the LWA used in our measurements, this results in the values shown in Table III. The radiation patterns of two sectors along with their approximation are shown in Fig. 10. As evident, the approximation fits very well for the main beam.

TSLS is furthermore parameterized to take into account the strong multipath environment. For heavy multipath, sectors far from the line-of-sight direction to the TX can be expected to be dominated by multipath components. Hence, we chose to use only $L = 3$ sectors in TSLS DoA estimation. Moreover, PW is chosen as the DoA fusion method since it is more robust than VW, which has been derived for a free space propagation, while generally having better performance than EW. For simplicity,

TABLE IV
PRACTICAL MEASUREMENT RESULTS

(a) Absolute error of DoA estimation.

	RX1	RX2	RX3	RX4	RX5	RX6	RMSE
TX1	18.5°	29.6°	5.3°	17.0°	21.9°	3.3°	18.4°
TX2	16.3°	21.3°	9.5°	0.6°	6.3°	2.2°	11.9°
TX3	23.1°	14.5°	8.0°	24.1°	26.6°	30.2°	22.4°
RMSE	19.5°	22.6°	7.8°	17.0°	20.2°	17.6°	

(b) Localization error after Stansfield fusion of DoA estimates.

	TX1 (TSLS)	TX2 (TSLS)	TX3 (TSLS)	RMSE (TSLS)	RMSE (maxE [31])
Absolute error	0.6 m	0.6 m	2.4 m	1.5 m	2.8 m

we estimate the RSSs for Stansfield weighting simply as the maximum NCSP of the MASP (see Section III-B and A) at RX k, $k = 1, \ldots, K$, i.e., $\hat{\gamma}_k = \max(p_{k,q}, p_{k,q+1})$.

C. Measured Performance

Table IV(a) presents the DoA estimation errors stemming from the processing of the measurements with the above described TSLS configuration. Based on these results, we recognize clear differences in the DoA estimation accuracy at different RXs. RX3 performs very well with all TXs and reaches the lowest RMSE due to its good coverage and interference-free location. In contrast to that, RX2 yields a relatively high DoA estimation RMSE. There is no obvious geometrical reason for that. However, one of the active WiFi hotspots was located right behind the wall close to RX2 and may thus have negatively influenced the estimation performance. The highest individual estimation error of 30.2° was obtained for the TX3-RX6 combination, which might have been caused by the rich scattering conditions due to the stairs (made of metal, concrete and glass) in proximity of RX6.

When analyzing the results in Table IV(a) row-wise, we see that the DoA of TX3 is the most difficult to estimate, as expected due to TX3's relatively isolated location. Moreover, TX3 was the node closest to the walls with metal doors on either side. We suspect that this caused strong multipath, contributing further to the large DoA estimation error. Surprisingly, TX2 turns out to have the most accurate DoA estimates even though it is located close to the stairs which might act as local scatterers. Actually, only two out of six DoA estimation errors of TX2 are in excess of 10°, meaning that TSLS provides very accurate estimates in this case. Overall, these results reveal that the TSLS algorithm is capable of estimating DoAs with fairly high accuracy even in a challenging indoor environment with severe multipath.

Fig. 9 depicts the TX location estimates resulting from the above described combination of TSLS DoA estimation with subsequent Stansfield localization. A detailed summary of the localization results is shown in Table IV(b). Based on these results, TX1 and TX2 can be localized very precisely as the location error is around 60 cm for both. This is an expected result due to their central locations with respect to the RXs. Although some of the individual DoA estimates have a comparably large error, location estimation is fairly accurate, which is mainly explained by the Stansfield weighting scheme that gives larger weight to the DoA estimates of those RXs that have large sector-powers. In case of TX3, the majority of the DoA estimates are relatively inaccurate with four out of six estimation errors being larger than 20°. Consequently, the location estimate is also more inaccurate (2.4 m). However, this is explained by the location of TX3 which was on purpose placed at the boarder of the localization system's coverage area.

The total localization RMSE is 1.5 m, which corresponds to a circle with an area of 2.1% of the whole measurement area. In our earlier work [31], we have used the same measurement data to test the performance of the modified maxE DoA estimator [31]. Using the same Stansfield fusion algorithm, but in combination with simple maxE DoA estimates resulted in a RMSE of 2.8 m, which is an almost two-fold RMSE compared to the localization based on TSLS DoA estimates. Hence the algorithms proposed in this article are clearly outperforming the existing state-of-the-art.

VIII. CONCLUSION

In this paper, we have substantially extended our earlier work on DoA estimation and TX localization using sectorized antennas. We have introduced a modified antenna model with more degrees of freedom and have shown that it can be used to model a broader range of practical antennas. Based on the new model we have proposed the novel TSLS DoA estimator. In contrast to existing DoA estimators, TSLS is applicable to all antennas that can be described by our modified antenna model, independent of the TX signal type and without the requirement for cooperation between the TX and the localizing network. Besides being more universal, we have shown that TSLS has also better performance than existing algorithms and that it approaches the CRB on signal DoA estimation of a non-cooperative TX if the SNR is moderate to large. In order to better understand the performance of TSLS, we have furthermore derived analytical error models for the underlying DoA estimation principle of TSLS DoA estimation considering free space as well as multipath propagation. We have then analyzed the performance of localization with the Stansfield estimator that estimates the TX location by fusing the TSLS DoA estimates. As expected, the improved DoA estimation performance of TSLS also results in a localization performance improvement compared to the localization using previously published DoA estimators. Finally, we have shown how to configure the TSLS DoA estimator to work with a practical sectorized antenna, namely a leaky-wave antenna. Based on that configuration we have then demonstrated the achievable performance of a sectorized antenna-based localization system using real-world measurements obtained in an indoor environment. Overall, we believe that the results in this paper are crucial for the practical implementation of low complexity DoA estimation and TX localization using sectorized antenna systems. In particular this is the case when the TX is non-cooperative or when dedicated signaling between TX and localization network is otherwise unfeasible.

APPENDIX A
DERIVATION OF DOA ESTIMATORS

The criterion (6) is clearly minimized for $p_{k,i}/p_{k,j} - \rho_{k,i}/\rho_{k,i} = 0$. Recalling the Gaussian approximation $\rho_{k,m} = [\zeta_m(\varphi_k)]^2$, $m = i, j$ in (1), we can write

$$0 = \ln\frac{p_{k,i}}{p_{k,j}} - 2\ln\frac{\alpha_i}{\alpha_j} + \frac{2\left[\mathcal{M}(\hat{\varphi}_{k,ij} - \vartheta_i)\right]^2}{\beta_i^2} - \frac{2\left[\mathcal{M}(\hat{\varphi}_{k,ij} - \vartheta_j)\right]^2}{\beta_j^2}. \quad (28)$$

The above equation contains the function $\mathcal{M}(\varphi)$, which is difficult to handle mathematically. However, the mapping of the angles to $[-\pi; \pi)$ is arbitrary. Hence, for practically relevant cases we can always find a mapping for the angles ϑ_i and ϑ_j such that we can write $\mathcal{M}(\hat{\varphi}_k - \vartheta_m) = \tilde{\varphi}_{k,ij} - \tilde{\vartheta}_m$, where $m = i, j$ and $\tilde{\varphi}_{k,ij}$ is the mapped SP-DoA estimate. One such mapping could be $\tilde{\vartheta}_i = 0$ and $\tilde{\vartheta}_j = \vartheta_j - \vartheta_i$. We can then solve (28) to obtain (7) and (8). For presentation simplicity, we have not included the mapping in (7) and (8).

APPENDIX B
PROOF OF LEMMA 1

In the following we will derive the mean (14) and variance (16) for the 2nd order Taylor series expansion. The 2nd order Taylor series of Y in Lemma 1 around its mean $\boldsymbol{\mu}$ can be written as

$$Y^{(2)} = f + \mathbf{j}^T(\mathbf{X} - \boldsymbol{\mu}) + \frac{1}{2}(\mathbf{X} - \boldsymbol{\mu})^T\mathbf{H}(\mathbf{X} - \boldsymbol{\mu}) \quad (29)$$

where we have omitted the dependence of f, $\mathbf{j}$ and $\mathbf{H}$ on $\boldsymbol{\mu}$ for notational simplicity. According to [33, p. 53], the moments of a quadratic form $V' = \mathbf{X}^T\mathbf{A}\mathbf{X}$ for normally distributed random vector $\mathbf{X} \sim \mathcal{N}(\boldsymbol{\mu}, \mathbf{Q})$ with symmetric matrix $\mathbf{A}$ are given as

$$\mathrm{E}[V'] = \mathrm{trace}(\mathbf{A}\mathbf{Q}) + \boldsymbol{\mu}^T\mathbf{A}\boldsymbol{\mu} \quad (30)$$

$$\mathrm{E}[V'^2] = 2\left[\mathrm{trace}(\mathbf{A}\mathbf{Q})^2 + 2\boldsymbol{\mu}^T\mathbf{A}\mathbf{Q}\mathbf{A}\boldsymbol{\mu}\right] \quad (31)$$

$$+ \left[\mathrm{trace}(\mathbf{A}\mathbf{Q}) + \boldsymbol{\mu}^T\mathbf{A}\boldsymbol{\mu}\right]^2. \quad (32)$$

In (29), we have $V = \Delta\mathbf{X}^T\mathbf{H}\Delta\mathbf{X}$ with $\Delta\mathbf{X} = \mathbf{X} - \boldsymbol{\mu} \sim \mathcal{N}(\mathbf{0}, \mathbf{Q})$ and the Hermitian matrix $\mathbf{H}$ that is consequently symmetric. We can therefore write the moments of V as

$$\mathrm{E}[V] = \mathrm{trace}(\mathbf{H}\mathbf{Q}) \quad (33)$$

$$\mathrm{E}[V^2] = 2\mathrm{trace}(\mathbf{H}\mathbf{Q})^2 + [\mathrm{trace}(\mathbf{H}\mathbf{Q})]^2. \quad (34)$$

Hence, the first moment of Y is obtained as in (14). The variance of Y can be written as

$$\begin{aligned}\mathrm{var}\left[Y^{(2)}\right] &= \mathrm{E}\left[\left(Y^{(2)}\right)^2\right] - \mathrm{E}\left[Y^{(2)}\right]^2 \\ &= \mathrm{E}[f^2] + \mathrm{E}\left[(\mathbf{j}^T\Delta\mathbf{X})^2\right] + \frac{1}{4}\mathrm{E}[V^2] \\ &\quad + 2f\mathbf{j}^T\mathrm{E}[\Delta\mathbf{X}] + f\mathrm{E}[V] + \mathbf{j}^T\mathrm{E}[\Delta\mathbf{X}V] \\ &\quad - f^2 - f\mathrm{trace}\{\mathbf{H}\mathbf{Q}\} - \frac{1}{4}[\mathrm{trace}(\mathbf{H}\mathbf{Q})]^2. \quad (35)\end{aligned}$$

We notice that $\Delta\mathbf{X}V$ is a vector with elements composed of products $\Delta\mathbf{X}_k^p\Delta\mathbf{X}_l^q\Delta\mathbf{X}_m^r$, where $\Delta\mathbf{X}_k$, $\Delta\mathbf{X}_l$ and $\Delta\mathbf{X}_m$ are independent and at least one of the powers p, q or r is uneven. Therefore, we have $\mathrm{E}[\Delta\mathbf{X}V] = 0$ and obtain (16) by using (33), (34) in (35). The corresponding mean (13) and variance (15) of the 1st order Taylor series are not derived explicitly, due to space constraints. However, the derivation is very similar.

APPENDIX C
DERIVATION OF SP-DOA ESTIMATION BIAS AND VARIANCE

For SP-DoA estimation with DBS, we have $\hat{\varphi}_{ij} = f(\mathbf{p}) = \lambda_{ij} \pm b_{ij}g(\mathbf{p})$ with $\mathbf{p} = (p_{k,i}, p_{k,j})^T$. This leads to the 2×1 gradient vector $\mathbf{j}$ with elements

$$\mathbf{j}_1 = [f]_{p_{k,i}}(\boldsymbol{\mu}) = \pm\frac{\beta_i\beta_j}{4p_{k,i}g(\boldsymbol{\mu})} \quad (36)$$

$$\mathbf{j}_2 = [f]_{p_{k,i}}(\boldsymbol{\mu}) = \mp\frac{\beta_i\beta_j}{4p_{k,j}g(\boldsymbol{\mu})} \quad (37)$$

and the 2×2 Hessian matrix $\mathbf{H}$ with elements

$$\mathbf{H}_{11} = [f]_{p_{k,i}p_{k,i}}(\boldsymbol{\mu}) = \mp\beta_i\beta_j\frac{4\left[g(\boldsymbol{\mu})\right]^2 + \Delta\beta_{ij}}{16p_{k,i}^2\left[g(\boldsymbol{\mu})\right]^3} \quad (38)$$

$$\mathbf{H}_{22} = [f]_{p_{k,j}p_{k,j}}(\boldsymbol{\mu}) = \pm\beta_i\beta_j\frac{4\left[g(\boldsymbol{\mu})\right]^2 - \Delta\beta_{ij}}{16p_{k,j}^2\left[g(\boldsymbol{\mu})\right]^3} \quad (39)$$

$$\mathbf{H}_{12} = \mathbf{H}_{21} = [f]_{p_{k,i}p_{k,j}}(\boldsymbol{\mu}) = \pm\frac{\beta_i\beta_j\Delta\beta_{ij}}{16p_{k,i}p_{k,j}\left[g(\boldsymbol{\mu})\right]^3} \quad (40)$$

both evaluated at $\mathbf{p} = \boldsymbol{\mu}$. We furthermore obtain

$$\mathrm{trace}(\mathbf{H}\mathbf{Q}) = \mathbf{H}_{11}\sigma_1^2 + \mathbf{H}_{22}\sigma_2^2 \quad (41)$$

$$\mathrm{trace}(\mathbf{H}\mathbf{Q})^2 = \left(\mathbf{H}_{11}\sigma_1^2\right)^2 + 2\mathbf{H}_{12}^2\sigma_1^2\sigma_2^2 + \left(\mathbf{H}_{22}\sigma_2^2\right)^2. \quad (42)$$

since $\mathbf{Q}$ is diagonal. Inserting (38)–(40) in (41) and using (41) in (14) yields $\mathrm{E}[\hat{\varphi}_{k,ij}^{(2)}]$ and, after subtraction of the DoA φ_k, the bias (18). (19) results from (15) and (36)–(37). Finally, inserting (42) in (16) and using the results from (19) leads to (20).

REFERENCES

[1] L. Kaplan, "Global node selection for localization in a distributed sensor network," *IEEE Trans. Aerosp. Electron. Syst.*, vol. 42, no. 1, pp. 113–135, Jan. 2006.
[2] H. Celebi and H. Arslan, "Utilization of location information in cognitive wireless networks," *IEEE Wireless Commun. Mag.*, vol. 14, no. 4, pp. 6–13, Aug. 2007.
[3] K. Ho and Y. Chan, "Solution and performance analysis of geolocation by TDOA," *IEEE Trans. Aerosp. Electron. Syst.*, vol. 29, no. 4, pp. 1311–1322, Oct. 1993.
[4] A. Weiss, "On the accuracy of a cellular location system based on RSS measurements," *IEEE Trans. Veh. Technol.*, vol. 52, no. 6, pp. 1508–1518, Nov. 2003.
[5] R. Martin and R. Thomas, "Algorithms and bounds for estimating location, directionality, and environmental parameters of primary spectrum users," *IEEE Trans. Wireless Commun.*, vol. 8, no. 11, pp. 5692–5701, Nov. 2009.

[6] F. Penna and D. Cabric, "Bounds and tradeoffs for cooperative DoA-only localization of primary users," in *Proc. IEEE GLOBECOM*, 2011, pp. 1–5.
[7] J. Wang, J. Chen, and D. Cabric, "Cramer–Rao bounds for joint RSS/DoA-based primary-user localization in cognitive radio networks," *IEEE Trans. Wireless Commun.*, vol. 12, no. 3, pp. 1363–1375, Mar. 2013.
[8] J. Werner, A. Hakkarainen, and M. Valkama, "Cramer–Rao bounds for hybrid RSS-DOA based location and transmit power estimation in cognitive radio systems," in *Proc. IEEE 78th VTC Fall*, 2013, pp. 1–7.
[9] R. Schmidt, "Multiple emitter location and signal parameter estimation," *IEEE Trans. Antennas Propag.*, vol. 34, no. 3, pp. 276–280, Mar. 1986.
[10] T. Ohira, "Adaptive array antenna beamforming architectures as viewed by a microwave circuit designer," in *Proc. Asia-Pac. Microw. Conf.*, 2000, pp. 828–833.
[11] J. Werner, J. Wang, A. Hakkarainen, M. Valkama, and D. Cabric, "Primary user localization in cognitive radio networks using sectorized antennas," in *Proc. 10th Annu. Conf. WONS*, 2013, pp. 155–161.
[12] J. Werner, J. Wang, A. Hakkarainen, M. Valkama, and D. Cabric, "Primary user DoA and RSS estimation in cognitive radio networks using sectorized antennas," in *Proc. 8th Int. Conf. CROWNCOM*, 2013, pp. 43–48.
[13] J. Wang, J. Werner, M. Valkama, and D. Cabric, "Performance analysis of primary user RSS/DoA estimation and localization in cognitive radio networks using sectorized antennas," *IEEE Wireless Commun. Lett.*, vol. 3, no. 2, pp. 237–240, Apr. 2014.
[14] D. Piazza, D. Michele, and K. Dandekar, "Two port reconfigurable CRLH leaky wave antenna with improved impedance matching and beam tuning," in *Proc. 3rd EuCAP*, 2009, pp. 2046–2049.
[15] C. Sun and N. C. Karmakar, "Direction of arrival estimation with a novel single-port smart antenna," *EURASIP J. Adv. Signal Process.*, vol. 2004, no. 9, pp. 1364–1375, Aug. 2004.
[16] K. Gotsis, K. Siakavara, and J. Sahalos, "On the direction of arrival (DoA) estimation for a switched-beam antenna system using neural networks," *IEEE Trans. Antennas Propag.*, vol. 57, no. 5, pp. 1399–1411, May 2009.
[17] M. Sharawi, F. Sultan, and D. Aloi, "An 8-element printed v-shaped circular antenna array for power-based vehicular localization," *IEEE Antennas Wireless Propag. Lett.*, vol. 11, pp. 1133–1136, Sep. 2012.
[18] M. S. Sharawi, F. Sultan, and D. N. Aloi, "A comparative performance analysis of two printed circular arrays for power-based vehicle localization applications," *Int. J. Antennas Propag.*, vol. 2012, Sep. 2012, Art. ID. 567918.
[19] X. Yu and H. Xin, "Direction of arrival estimation utilizing incident angle dependent spectra," in *Proc. IEEE MTT-S Int. Microw. Symp. Dig.*, 2012, pp. 1–3.
[20] V. Vakilian, J.-F. Frigon, and S. Roy, "Direction-of-arrival estimation in a clustered channel model," in *Proc. IEEE 10th Int. NEWCAS*, 2012, pp. 313–316.
[21] H. Paaso, A. Mammela, D. Patron, and K. R. Dandekar, "DoA estimation through modified unitary MUSIC algorithm for CRLH leaky-wave antennas," in *Proc. IEEE 24th Int. Symp. PIMRC*, 2013, pp. 311–315.
[22] D. N. Aloi and M. S. Sharawi, "Comparative analysis of single-channel direction finding algorithms for automotive applications at 2400 MHz in a complex reflecting environment," *Phys. Commun. J.*, vol. 3, no. 1, pp. 19–27, Mar. 2010.
[23] M. S. Sharawi and D. N. Aloi, "Characterizing the performance of single-channel pseudo-doppler direction finding systems at 915 MHz for vehicle localization," *Int. J. Commun. Syst.*, vol. 24, no. 1, pp. 27–39, Jan. 2011.
[24] S. Abielmona, H. Nguyen, and C. Caloz, "Analog direction of arrival estimation using an electronically-scanned CRLH leaky-wave antenna," *IEEE Trans. Antennas Propag.*, vol. 59, no. 4, pp. 1408–1412, Apr. 2011.
[25] T. Ohira and K. Gyoda, "Hand-held microwave direction-of-arrival finder based on varactor-tuned analog aerial beamforming," in *Proc. Asia-Pac. Microw. Conf.*, 2001, pp. 585–588.
[26] F. Gunnarsson *et al.*, "Downtilted base station antennas—A simulation model proposal and impact on HSPA and LTE performance," in *Proc. IEEE 68th Vehicular Technology Conf., VTC* Fall, Sept. 2008, pp. 1–5.
[27] *Evolved Universal Terrestrical Radio Access (E-UTRA)*, 3GPP TR 25.814 V. 7.10, 2011.
[28] R. Stansfield, "Statistical theory of D.F. fixing," *J. Inst. Elect. Eng.—IIIA: Radiocommun.*, vol. 94, no. 15, pp. 762–770, Mar. 1947.
[29] J. Werner, J. Wang, A. Hakkarainen, M. Valkama, and D. Cabric, "Performance and Cramer-Rao bounds for DoA/RSS estimation and transmitter localization using sectorized antennas," *IEEE Trans. Veh. Technol.*, accepted for publication.
[30] N. I. Fisher and T. Lewis, "Estimating the common mean direction of several circular or spherical distributions with differing dispersions," *Biometrika*, vol. 70, no. 2, pp. 333–341, Aug. 1983.
[31] A. Hakkarainen *et al.*, "Reconfigurable antenna based DoA estimation and localization in cognitive radios: Low complexity algorithms and practical measurements," in *Proc. 9th Int. Conf. CROWNCOM*, 2014, pp. 454–459.
[32] Mango Communications WARP v3 Kit, 2014. [Online]. Available: http://mangocomm.com/products/kits/warp-v3-kit
[33] A. M. Mathai and S. B. Provost, *Quadratic Forms in Random Variables: Theory and Applications*, 1st ed. New York, NY, USA: Marcel Dekker, 1992.

Janis Werner (S'14) was born in Berlin, Germany, in 1986. He received the Dipl.Ing. degree in electrical engineering from Dresden University of Technology (TUD), Germany, in 2011. Currently, he is working towards the Ph.D. degree at Tampere University of Technology (TUT), Finland, where he is a Researcher with the Department of Electronics and Communications Engineering. His main research interests are localization with an emphasis on directional antenna-based systems as well as the utilization and further processing of location information in future generation mobile networks.

Jun Wang received the B.Eng. degree in electronic information engineering from Beijing University of Technology and the M.Phil. degree in electrical engineering from City University of Hong Kong, in 2006 and 2009, respectively. He received the Ph.D. degree in electrical engineering from the University of California, Los Angeles, CA, USA, in 2014, advised by Prof. Danijela Cabric. He joined Broadcom Corporation as a Research Scientist in wireless communication systems design in 2014. His research interests include acquisition and utilization of primary-user location information and various issues related to spectrum sensing in cognitive radio networks.

Aki Hakkarainen (S'14) received the M.Sc. degree (with honors) in communication electronics from Tampere University of Technology (TUT), Finland, in 2007. From 2007 to 2009, he was a RF Design Engineer with Nokia, Salo. From 2009 to 2011, he was a Radio System Specialist with Elisa, Tampere. Currently, he is working towards the Ph.D. degree at TUT. He is a Researcher and Doctoral Student with the Department of Electronics and Communications Engineering, TUT. His research interests include digital signal processing methods for RF impairment mitigation and digital signal processing for localization.

Nikhil Gulati (S'07) received the B.Eng. degree in electronics instrumentation and control from the University of Rajasthan, India, in 2005 and the M.S. degree in electrical engineering with a major in systems and control from Drexel University, Philadelphia, PA, USA, in 2007, where he conducted research on sensor networks, autonomous systems and real-time control. He is currently pursuing the Ph.D. degree in electrical engineering at Drexel University. He worked as a Software Engineer from 2007–2010. His research is focused on developing adaptive learning algorithms for cognitive radios employing electrical reconfigurable antennas. He also works on developing distributed algorithms for interference management and heterogeneous wireless networks.

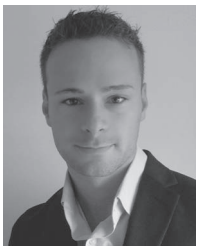

Damiano Patron (S'15) received the B.S. degree in electronics engineering from University of Padua, Italy, in 2010 and the M.S. degree in electrical and computer engineering from Drexel University, Philadelphia, PA, USA, in 2013, where he is currently pursuing the Ph.D. degree in telecommunication engineering. From 2002 to 2010, he worked with Euro-Link S.r.l. as a System Integrator of RFID systems. In 2010, he joined the start-up company Adant Inc. as an RF and Antenna Engineer, designing reconfigurable antennas for WiFi and RFID applications. His research focuses on the design of reconfigurable antennas for throughput maximization and DoA estimation in wireless networks. He also works in the development of wearable sensors and power harvesting systems. He is the author and coauthor of several patents in the field of reconfigurable antennas, antennas miniaturization and wearable technologies. He received several awards including the Drexel Frank and Agnes Seaman Fellowship Award in 2013 and the Young Scientist Best Paper Award at the ICEAA—IEEE APWC—EMS 2013 Conference.

Doug Pfeil received the B.S. and M.S. degrees in computer engineering in 2007 from Drexel University, Philadelphia, PA, USA. He is currently pursuing the Ph.D. degree from Drexel University where he is also a member of the research staff in the Wireless Systems Lab. His current research interests include software defined radio, free space optical communication, physical layer design, and FPGA baseband processing with an emphasis on the practical implementation of novel hybrid RF and optical communication techniques.

Kapil Dandekar (S'95–M'01–SM'07) received the B.S. degree in electrical engineering from the University of Virginia in 1997, and the M.S. and Ph.D. degrees in electrical and computer engineering from the University of Texas at Austin in 1998 and 2001, respectively. In 1992, he worked at the U.S. Naval Observatory and from 1993-1997 he worked at the U.S. Naval Research Laboratory.

In 2001, he joined the Electrical and Computer Engineering Department, Drexel University, Philadelphia, PA, USA. He is currently a Professor of Electrical and Computer Engineering at Drexel University; the Director of the Drexel Wireless Systems Laboratory (DWSL); Associate Dean for Research and Graduate Studies in the Drexel University College of Engineering. DWSL has been supported by the U.S. National Science Foundation, Army CERDEC, National Security Agency, Office of Naval Research, and private industry. His current research interests and publications involve wireless, ultrasonic, and optical communications, reconfigurable antennas, and smart textiles. Intellectual property from DWSL has been licensed by external companies for commercialization. He is a member of the IEEE Educational Activities Board and co-founder of the EPICS-in-IEEE program.

Danijela Cabric (S'02–M'07–SM'14) received the Dipl. Ing. degree from the University of Belgrade, Serbia, in 1998, and the M.Sc. degree in electrical engineering from the University of California, Los Angeles, CA, USA, in 2001. She received the Ph.D. degree in electrical engineering from the University of California, Berkeley, CA, USA, in 2007, where she was a member of the Berkeley Wireless Research Center. In 2008, she joined the faculty of the Electrical Engineering Department, University of California, Los Angeles, where she is now Associate Professor. She received the Samueli Fellowship in 2008, the Okawa Foundation Research Grant in 2009, Hellman Fellowship in 2012 and the National Science Foundation Faculty Early Career Development (CAREER) Award in 2012. She serves as an Associate Editor for the IEEE JOURNAL ON SELECTED AREAS IN COMMUNICATIONS (Cognitive Radio series) and IEEE COMMUNICATIONS LETTERS, and TPC Co-Chair of 8th International Conference on Cognitive Radio Oriented Wireless Networks (CROWNCOM) 2013. Her research interests include novel radio architecture, signal processing, and networking techniques to implement spectrum sensing functionality in cognitive radios.

Mikko Valkama (S'00–M'01) was born in Pirkkala, Finland, on November 27, 1975. He received the M.Sc. and Ph.D. degrees (both with honors) in electrical engineering (EE) from Tampere University of Technology (TUT), Finland, in 2000 and 2001, respectively. In 2002, he received the Best Ph.D. Thesis award by the Finnish Academy of Science and Letters for his dissertation entitled "Advanced I/Q signal processing for wideband receivers: Models and algorithms". In 2003, he was working as a Visiting Researcher with the Communications Systems and Signal Processing Institute, SDSU, San Diego, CA, USA. Currently, he is a Full Professor and Department Vice-Head at the Department of Electronics and Communications Engineering, TUT, Finland. He has been involved in organizing conferences, like the IEEE SPAWC'07 (Publications Chair) held in Helsinki, Finland. His general research interests include communications signal processing, estimation and detection techniques, signal processing algorithms for software defined flexible radios, cognitive radio, full-duplex radio, radio localization, 5G mobile cellular radio, digital transmission techniques such as different variants of multicarrier modulation methods and OFDM, and radio resource management for ad-hoc and mobile networks.